Slanted snaking of localized Faraday waves

Bastián Pradenas, Isidora Araya, Marcel G. Clerc, and Claudio Falcón[*]
Departamento de Física, Facultad de Ciencias Físicas y Matemáticas, Universidad de Chile, Casilla 487-3, Santiago, Chile

Punit Gandhi
Mathematical Biosciences Institute, The Ohio State University, Columbus, Ohio 43210, USA

Edgar Knobloch[†]
Department of Physics, University of California at Berkeley, Berkeley, California 94720, USA
(Received 2 September 2016; published 21 June 2017)

We report on an experimental, theoretical, and numerical study of slanted snaking of spatially localized parametrically excited waves on the surface of a water-surfactant mixture in a Hele-Shaw cell. We demonstrate experimentally the presence of a hysteretic transition to spatially extended parametrically excited surface waves when the acceleration amplitude is varied, as well as the presence of spatially localized waves exhibiting slanted snaking. The latter extend outside the hysteresis loop. We attribute this behavior to the presence of a conserved quantity, the liquid volume trapped within the meniscus, and introduce a universal model based on symmetry arguments, which couples the wave amplitude with such a conserved quantity. The model captures both the observed slanted snaking and the presence of localized waves outside the hysteresis loop, as demonstrated by numerical integration of the model equations.

DOI: 10.1103/PhysRevFluids.2.064401

I. INTRODUCTION

Dissipative systems driven out of equilibrium display spatial patterns that can extend over the whole system or be confined to a localized region [1–3]. Examples of the latter include dissipative solitons, fronts, and localized oscillations called oscillons [3] and these have been observed in a great variety of physical systems ranging from simple and complex fluids to liquid crystals, chemical reactions, magnetic materials, granular media, and elastic solids. The theoretical understanding of these structures is largely based on detailed studies of the bistable Swift-Hohenberg equation [4], although geometrical methods have been successfully applied to one-dimensional systems [5,6]. This understanding centers on the presence of a pinning mechanism [7] whereby fronts connecting a homogeneous state to a spatially structured state pin to the latter, resulting in the presence of stationary fronts even at parameter values away from the Maxwell point at which the structured state has the same energy as the competing homogeneous state [3]. The theory shows that the resulting pinning region contains an infinite number of coexisting localized states organized in a snakes-and-ladders structure straddling the Maxwell point [8,9]. Such states are therefore located within the hysteresis loop between the homogeneous and structured states. For steady localized states the corresponding bifurcation diagrams can take the form of standard snaking [4] in which different length states all coexist within a pinning region, or their intervals of existence may be staggered generating slanted snaking [10–15], an effect attributed to nonlocality [16,17]. Neither type of structure has thus far been reported in experiments on localized standing oscillations, even though such oscillations are

[*]cfalcon@ing.uchile.cl
[†]knobloch@berkeley.edu

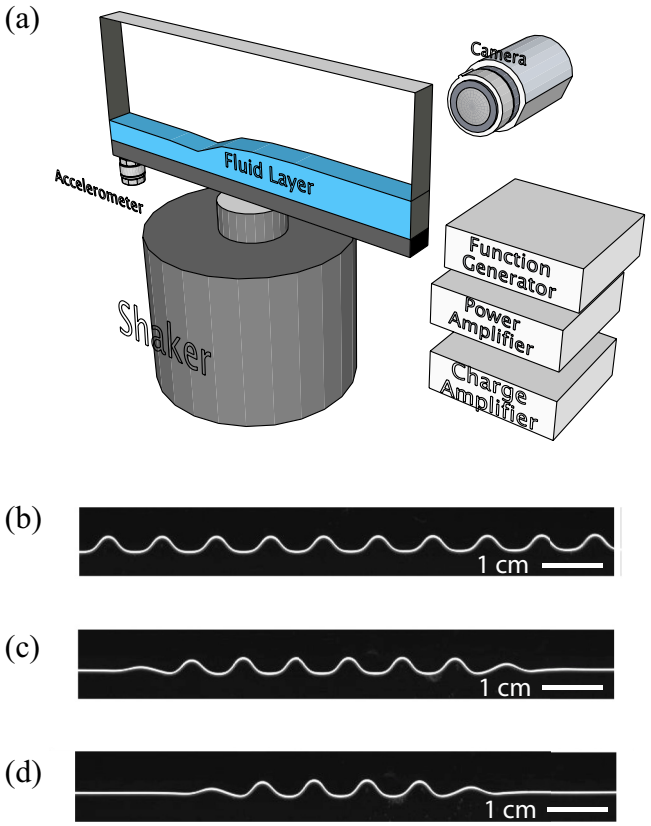

FIG. 1. (a) Experimental setup showing a glass cell on a shaker. (b) Spatially extended Faraday wave. (c) Spatially localized Faraday wave with $n = 8$ peaks. (d) Spatially localized Faraday wave with $n = 6$ peaks. In (b)–(d) only a part of the whole domain is shown.

known to be present within the hysteresis loop between extended standing waves and a homogeneous state [18–20].

In this paper we demonstrate slanted snaking of localized oscillations in a Faraday wave experiment [21], specifically waves at the surface of a water-surfactant mixture held between two-plates in a Hele-Shaw configuration and vibrated vertically. The extended wave pattern appears across the entire experimental cell through a subcritical instability that depends on the contact angle hysteresis of the triple line and the confinement width. Localized Faraday waves are observed both inside and outside the hysteresis loop between the extended pattern and the flat interface and display a snaking structure that is slanted. The organization of the observed localized oscillations can be understood using a pair of amplitude equations that capture the coupling between the amplitude of the parametrically excited standing waves and a long-wave conserved mode representing the volume of liquid trapped within the meniscus. Numerical simulations of the proposed coupled equations are in good qualitative agreement with theoretical predictions and experimental observations.

II. EXPERIMENTAL SETUP

The experimental setup is depicted in Fig. 1. Two glass plates are separated by an aluminum frame creating a glass container (width $w = 1$ mm, height $h = 40$ mm, and length $l = 200$ mm) that is filled to a height $h_0 = 23$ mm with a mixture of 85% distilled water and 15% surfactant (Kodak Photo-Flo2 200$^{\text{TM}}$) by volume. The width w and the height h_0 vary across the experimental cell by less than

5% and 1%, respectively. The density ρ of the working fluid is estimated at 1004 kg/m^3. Its surface tension σ was measured at 22 mN/m by the sessile drop method [22]. Its kinematic viscosity was measured at 3 ± 0.3 cSt using a stress-controlled rheometer (RheolabQC from Anton-Paar) at room temperature ($20\,^\circ\text{C} \pm 2\,^\circ\text{C}$) in a Couette configuration (inner diameter 19.39 mm, outer diameter 21.00 mm, and angle of the rotating cone 120°) for steady shear rates $\dot{\gamma} \in [40,100]\ \text{s}^{-1}$, as appropriate to our experiments. Normal stresses were not measured. The wetting angle of the fluid mixture on glass was measured between 5° and 15°, showing partial wetting and contact angle hysteresis [23]. The glass container with the working fluid was mounted vertically on an electromechanical shaker driven sinusoidally by a function generator via a power amplifier. The vertical modulation of the acceleration $a(t) = a\cos(\omega t)$ was monitored by a piezoelectric accelerometer via a charge amplifier. Horizontal accelerations were less than 1%. The experimental control parameter range was $a \in [2,20]$ m/s^2 and $f \equiv \omega/2\pi \in [30,60]$ Hz. For $f < 35$ Hz, no localized structures were found. In the present study we use $f = 45$ Hz, while a spans the whole experimental range.

Images of the surface profile are acquired with a CCD camera over a 10-s time window in a 1220×200 pixel spatial window (0.12-mm/pixel sensitivity in the horizontal direction and 0.11-mm/pixel sensitivity in the vertical direction). For each value of a, a sequence of images is taken at frequency $f/2$ using the second output of the function generator as a trigger to ensure a stroboscopic view of the oscillating surface profile. The profile of the fluid elevation $\eta(x,t) \equiv h(x,t) - h_0$ is tracked for every point x in space at each instant t using a simple threshold intensity algorithm [24], as shown in Fig. 1. To do this, white light is passed through a diffusing screen from behind the layer while images are taken from the front, enhancing contrast and improving the functioning of the surface tracking algorithm. Figure 1 shows snapshots of the layer displaying a spatially extended wave [Fig. 1(b)] and a spatially localized wave [Figs. 1(c) and 1(d)].

III. SPATIALLY LOCALIZED FARADAY WAVES

As we increase a above the critical value $a_c = 13.35$ m/s^2, the fluid layer becomes unstable to a parametric instability, displaying a stationary pattern of waves filling the entire experimental cell. Figure 1(b) shows a part of this state. The pattern oscillates at frequency $f/2$ with onset wavelength $\lambda = 9$ mm. The shape of the pattern is not symmetric with respect to the mean height: Cusps are sharp and troughs are smooth and flat (see Fig. 1). When a is decreased the extended pattern persists down to $a_{\text{fold}} = 10.5$ m/s$^2 < a_c$ where it collapses to the homogeneous flat state, indicating the presence of a hysteresis loop. To characterize the pattern evolution we compute the rms surface displacement $\langle \eta_\lambda \rangle \equiv \sqrt{\frac{\omega}{4\pi l}\int_0^l \int_0^{4\pi/\omega} \eta^2(x,t)\,dx\,dt}$. Figure 2(a) shows $\langle \eta_\lambda \rangle$ as a function of a for a variety of spatially extended and spatially localized states. The figure reveals a large hysteresis loop between the flat interface and a standing, spatially extended Faraday wave extending from a_c down to a_{fold}. We have confirmed that the hysteresis loop is reproducible by repeating the experimental procedure 5 times with a waiting time of 30 s between measurements.

Below a_{fold} our experimental system displays stable but localized Faraday waves [Fig. 2(b)]. These are created as follows. The acceleration is gradually decreased below $a = a_{\text{fold}}$. As one passes this critical acceleration the wave pattern detaches from one or other lateral boundary. A fully localized Faraday wave is then produced using a pin to drag the wave away from the other boundary. Once a stable, fully localized structure is obtained it remains in place and its extent in parameter space can be determined by gradually decreasing or increasing the acceleration a. This interval extends below $a = a_{\text{fold}}$. The localized structures generated in this manner are characterized by the number n of peaks within the pattern [Fig. 1(c)], with $n \in [5,N]$, where $N = 20$ is the number of peaks in the extended pattern. The existence intervals of these patterns depend on n, with patterns with consecutive values of n overlapping while shifting to larger values of a as n increases as in Fig. 2(b).

In Fig. 3 we show a superposition of three profiles with $n = 6,8,10$ peaks and pixel size resolution in the vertical. The figure shows that the profiles overlap in their center very precisely, indicating that this portion of the wave profile indeed corresponds to a portion of a periodic wave train. The

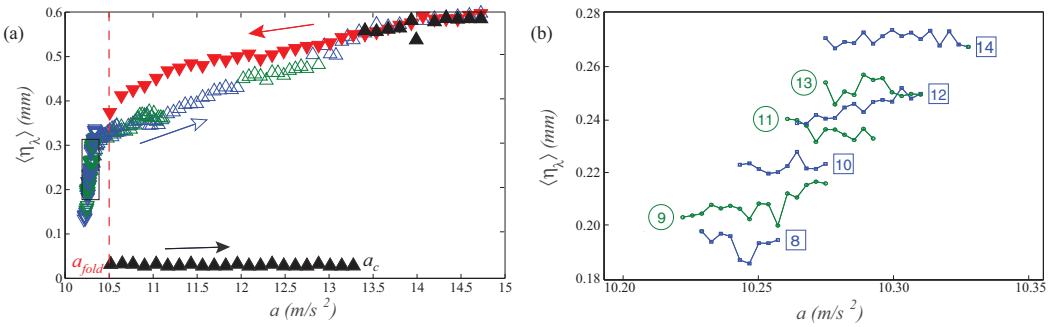

FIG. 2. (a) Experimental bifurcation diagram for a glass cell and increasing (▲) and decreasing (▼) acceleration a, displaying a hysteresis loop in the pattern amplitude $\langle \eta_\lambda \rangle$ between a_c and $a_{\rm fold}$. Localized structures for increasing (△) and decreasing (▽) a are also displayed. The colors correspond to even (blue) and odd (green) numbers of peaks n, $5 \leqslant n \leqslant 20$. (b) Detail of slanted snaking of localized structures outside the hysteresis loop [box in (a)] for n even (blue squares) and n odd (green circles) for $8 \leqslant n \leqslant 14$. The results are suggestive of intertwined branches of localized states with odd and even n exhibiting slanted snaking.

figure also reveals the spatial structure of the fronts connecting the pattern to the background state. We see that the liquid height in the background state is slightly asymmetric, at the level of a single pixel (0.1 mm) in 1000 pixels (100 mm) in the horizontal. In addition, this representation of the instantaneous wave profile reveals the effect of the lateral meniscus, which rises some 5 pixels (0.5 mm) above the background at $x = 0, l$. This lateral meniscus is present even when the localized waves are absent and is not responsible for the observed localization. The background asymmetry detected is at the level of the accuracy of our measurements and plays no role: The lateral meniscus prevents lateral motion that would take place in a slightly tilted apparatus in the absence lateral boundaries.

The presence of localized patterns outside the bistability region $a_{\rm fold} < a < a_c$ [both below $a_{\rm fold}$ and above a_c; see Fig. 2(a)] is the consequence of contact angle hysteresis at the front and back walls of the container. To probe this idea we have performed runs in plexiglass cells with the same $l = 200$ mm, $h = 40$ mm, and $h_0 = 23$ mm and different widths $w = 1$, 3, 5, and 8 mm. Plexiglass has different wetting properties than glass, thereby changing the values of a_c and $a_{\rm fold}$ for the same experimental cell parameters, but is easy to machine, allowing us to span a larger range of w. The bifurcation diagrams for these cells are shown in Fig. 4(a): As w increases the threshold a_c for the

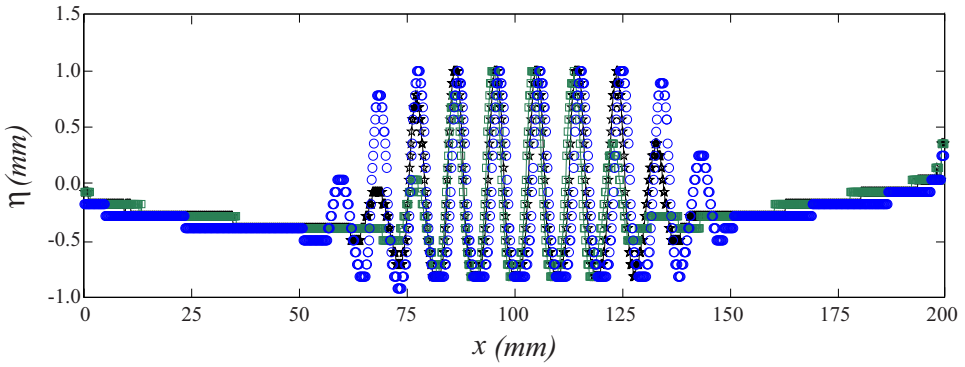

FIG. 3. Superposed profiles of coexisting localized Faraday waves with $n = 6, 8, 10$ peaks at $a = 10.27\,\mathrm{m/s^2}$ and identical temporal phase showing that the profiles match perfectly in the center and only differ in the location of the fronts on either side. The meniscus at $x = 0, l$ raises the height of the liquid at these locations by 0.5 mm over a distance of 100 mm.

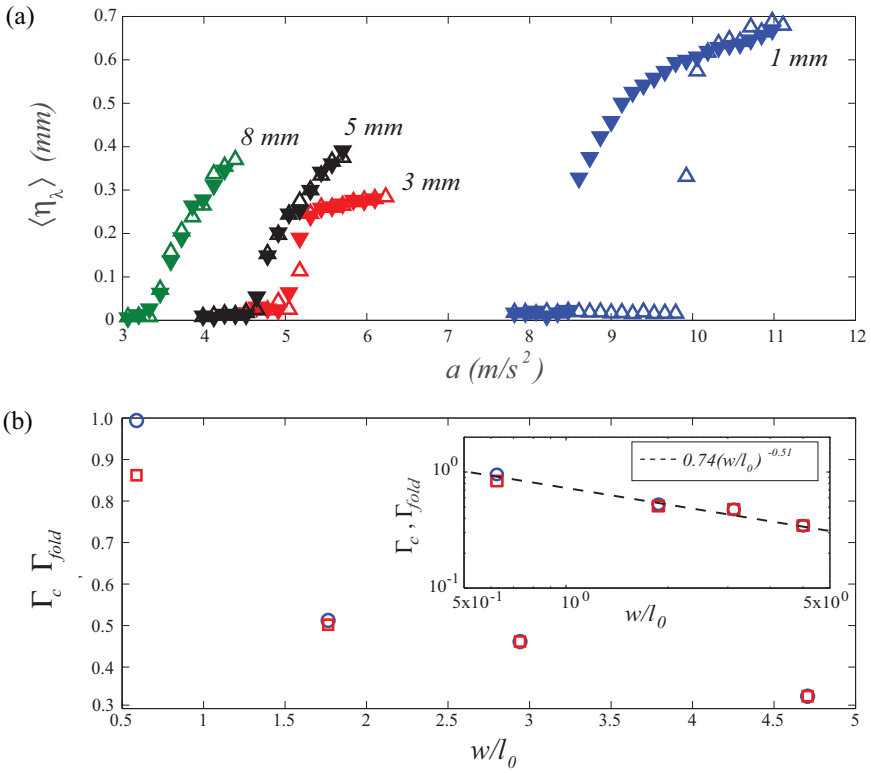

FIG. 4. (a) Experimental bifurcation diagrams for extended states in a plexiglass cell for increasing (△) and decreasing (▼) acceleration a when $w = 1$, 3, 5 and 8 mm. (b) Normalized acceleration at onset $\Gamma_c = a_c/g$ (○) and at the fold $\Gamma_{\rm fold} = a_{\rm fold}/g$ (□) as a function of the width w normalized by the capillary length $l_0 = 1.7$ mm. The inset shows a log-log plot of $\Gamma_c = a_c/g$ (○) and $\Gamma_{\rm fold} = a_{\rm fold}/g$ (□) as a function of w/l_0.

parametric instability and the lowest acceleration $a_{\rm fold}$ at which extended waves are still present both decrease [Fig. 4(b)] and for $w \gtrsim 3$ mm the hysteresis and the localized waves both disappear. The up-down asymmetry of the extended pattern also decreases (not shown).

IV. THEORETICAL INTERPRETATION

Slanted snaking of stationary localized states has been reported before [16,17,25] and was attributed to the presence of a conserved quantity [26,27], following earlier work of Matthews and Cox [28,29]; see also Ref. [30]. We believe that this is so also in the present case and conjecture that the conserved quantity responsible for slanted snaking in the present system is the volume of fluid trapped within the meniscus. The volume per unit length (i.e., the cross-sectional area) for a given meniscus height depends on the contact angle at the front and back walls and the associated contact angle hysteresis requires that fluid volume is redistributed along the length of the cell as the contact angle oscillates. The effect of this redistribution is more pronounced in a narrower cell because (i) confinement enhances contact angle hysteresis and (ii) the volume of liquid associated with this redistribution constitutes a larger change in height when averaged across the width of the cell (Fig. 4). We emphasize this point since the obvious conserved quantity characterizing the system, the *total* liquid volume, exerts an apparently negligible effect on the overall dynamics. Specifically, the presence of a wave generates a positive increase in the time-averaged local height, the so-called wave setup in hydraulics terminology. For spatially localized waves this increase in the effective

height of liquid must be compensated by a corresponding decrease in height outside the localized wave, an effect that is observed but cannot be reliably measured (the height decrease is $\sim 100\ \mu$m for localized structures with 5–8 bumps at the same a). We have checked that the corresponding increase in the time-averaged liquid height within the localized state exerts a negligible effect on the wavelength of the Faraday oscillations, as predicted from the (inviscid) dispersion relation. We emphasize that localized states, unlike spatially periodic oscillations, are free to adjust their wavelength since the cell sidewalls impose no constraint on their wavelength.

In view of this discussion we use the observation of slanted snaking in our system as evidence for the presence of a conserved quantity, most likely the liquid volume trapped within the meniscus. This volume is cycled in and out of the localized Faraday wave and represents therefore a fraction of the total volume that is exchanged between the wave and background. To understand more precisely how this works consider a wave with n crests at a given time $t = 0$. At time $t = 2\pi/\omega$, where ω is the forcing frequency, these crests become troughs and the troughs become crests. Since the structure is spatially localized this means that the $n - 1$ crests within the structure are identical to the those at $t = 0$ but there are now two additional crests on either side that are inevitably present, albeit smaller. Thus the state at $t = 2\pi/\omega$ must pull in water from the region outside the localized wave to supply the lengthened meniscus. This process then reverses and at $t = 4\pi/\omega$ the original state is recovered. Note that the volume of liquid that is exchanged between the wave and background is only a property of the fronts at either end of the structure and is therefore independent of the length of the structure. Thus the same volume is involved in each and every localized Faraday wave and the amount of volume involved only depends on the front profile and on the mean contact angle with the front and back walls. Thus, while the total volume of liquid does not change, the system nonetheless exhibits spatial modulation in the time-averaged volume $\overline{\Delta v}$ trapped within the meniscus (averaged over one oscillation period $0 < t < 4\pi/\omega$) and it is this conserved mode that couples to the localized pattern.

We now describe how we model the effects of this coupling. Since the volume of liquid involved spans the length of the localized wave it varies on a horizontal scale that is comparable to the length of the structure and hence formally much greater than the wavelength of the wave as predicted by the dispersion relation. Consequently, we treat this conserved mode as a long-wave mode $\overline{\Delta v}(X,T)$, where X and T are appropriate slow spatial and temporal scales, and propose an approach based on amplitude (or envelope) equations. These equations describe qualitatively the motion of the fluid surface as a standing wave appearing through a parametric instability coupled dynamically with a conserved quantity. Thus, we write the elevation of the liquid surface in the form

$$\eta(x,t) = [A(X,T)e^{ik_c x} + \bar{A}(X,T)e^{-ik_c x}]e^{i\omega t/2} + B(X,T) + \text{c.c.}, \tag{1}$$

where $A(X,T)$ is the (complex) amplitude of a surface wave oscillating with frequency $\omega/2$ at wave vector $k_c = k_c(\omega/2)$ and $B(X,T)$ is a (real) amplitude representing the effect on the time-averaged liquid height of the conserved volume $\overline{\Delta v}(X,T)$. The resulting expression is to be interpreted as describing the width-averaged data. Using symmetry arguments or multiscale analysis [27–29] and assuming that the group velocity of the waves is small, one finds that the simplest set of equations for the amplitudes A and B describing a parametric instability to standing waves coupled to a conserved mode takes the (scaled) form

$$A_T = (\mu + i\nu)A + \gamma\bar{A} + (1 + i\alpha)A_{XX} - (1 + i\beta)|A|^2 A + (\delta + i\sigma)BA, \tag{2}$$

$$B_T = B_{XX} - (|A|^2)_{XX}. \tag{3}$$

Equation (2) describes the long-time T and large-scale X evolution of the envelope $A(X,T)$ of a Faraday wave in a system that is parametrically driven near a 2:1 temporal resonance [31]. Here $\mu < 0$ represents the effects of viscous damping, ν corresponds to detuning between $\omega/2$ and the natural frequency of oscillation at wave number k_c, and α, β, and γ measure dispersion, the amplitude dependence of the frequency, and the magnitude of the time-periodic forcing, respectively. Constant nonzero values of B, $B = B_0$, describe the effect of changing the liquid volume trapped in

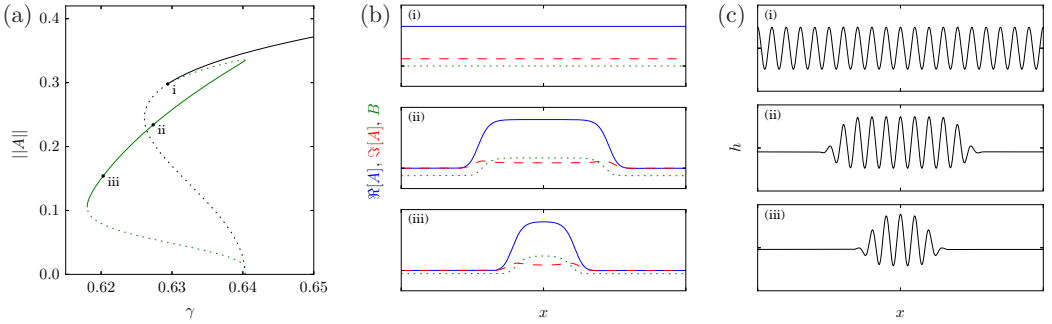

FIG. 5. (a) Numerical bifurcation diagram showing time-independent solutions of Eqs. (2) and (3). The homogeneous state (black) corresponds to a domain-filling Faraday wave, while the localized states (green) lie on a slanted branch. Stable (unstable) portions of the solution branches are drawn with solid (dotted) lines. (b) Profiles of the real (blue solid line) and imaginary (red dashed line) parts of the amplitude A and of the conserved mode B (green dotted line) for both localized and homogeneous states. (c) Profiles of the elevation $h(x,0)$ of the fluid surface relative to h_0 as predicted by Eq. (1); both odd and even states lie in the same branch. The parameters are $\mu = -0.5$, $\nu = 0.4$, $\alpha = 1$, $\beta = 2$, $\delta = 0.25$, $\sigma = 0$, and $\lambda_c = 1$.

the meniscus, thereby changing the decay rate of free oscillations (by shifting μ to $\mu + \delta B_0$) and the detuning (by shifting ν to $\nu + \sigma B_0$). In our experiment the trapped volume is fixed (i.e., $B = 0$ when the wave amplitude A is constant) but the B equation describes its redistribution in response to the presence of localized waves via the source term $(|A|^2)_{XX}$ arising from the presence of fronts between the Faraday wave and the flat background state. Since $B = 0$ for constant amplitude patterns the coupling to the large-scale mode does not affect extended Faraday waves or the threshold $a = a_c$ for the Faraday instability.

For stationary but spatially localized states the amplitude $A(X)$ satisfies the nonlocal equation

$$(1 + i\alpha)A_{XX} + (\mu + i\nu)A - (1 + i\beta)|A|^2 A + \gamma \bar{A} + (\delta + i\sigma)(|A|^2 - \langle |A|^2 \rangle)A = 0, \qquad (4)$$

where $\langle |A|^2 \rangle \equiv l^{-1} \int_{-l/2}^{l/2} |A|^2 dX$. The trivial $A = 0$ state corresponds to a flat surface with no pattern, while the constant amplitude state $A = A_0 \neq 0$ corresponds to a domain-filling Faraday wave. Localized Faraday waves are represented by time-independent states that consist of a section of the $A = A_0$ state embedded in an $A = 0$ background. In the absence of coupling to the large-scale mode ($\delta = \sigma = 0$) such states exist at a single value of γ. The coupling is responsible for effective dissipation that depends on the spatial extent of the localized state, thereby generating a slant in the branch of localized solutions as a function of the forcing strength γ: Broader solutions experience larger dissipation and require stronger forcing for their existence. Figure 5 shows stationary localized and domain-filling patterns predicted by the amplitude equations (2) and (3) and confirms that the model equations capture qualitatively not only the predicted slanting of the branch of localized states but also the profile of trapped liquid within the wave as measured by the B field. Note in particular that stable localized states extend slightly beyond the threshold for the primary instability, a feature that is also present in our experimental data [Fig. 2(a)].

Equations (2) and (3) describe small-amplitude states near onset of the Faraday instability on the assumption that the envelope of the pattern varies on a length scale that is much longer than the characteristic wavelength $2\pi/k_c$. The resulting separation of the spatial dependence of the solution into a dependence on slow and fast spatial scales eliminates pinning of the fronts on either side of the localized structure to the spatial oscillations within [4,7,19,32], thereby collapsing the branches of odd and even states into a single inclined nonsnaking branch. True snaking, such as that observed in our experiment, is only observed when terms beyond all orders are included in the amplitude equation [33] or, more usefully, in models in which the finite characteristic wave number k_c is built into the equation for the fluctuating part of the wave profile, $\eta(x,t) = H(x,t)\exp(i\omega t/2) + \text{c.c.}$ A

prototypical model of this type is provided by the parametrically forced complex Swift-Hohenberg equation [34,35]

$$H_t = (\mu + i\nu)H + i\zeta H_{xx} - (1 + i\alpha)\left(\partial_x^2 + k_c^2\right)^2 H + \gamma \bar{H} - (1 + i\beta)|H|^2 H + (\delta + i\sigma)BH \quad (5)$$

coupled to a conserved quantity as in Eq. (3). As shown in Fig. 6(a), odd and even localized solutions of this model do exhibit the type of intertwined slanted snaking observed in the experiment [Fig. 2(b)]. Larger values of the coupling parameter ζ increase the slanted snaking range and move it further outside the hysteresis loop [Fig. 6(a)], while lower values lead to a decrease in the snaking amplitude and ultimately to so-called smooth snaking [Fig. 6(e)] in which the successive folds in the snaking branches are absent [26,36]. However, in all cases the localized Faraday waves originate in a secondary bifurcation from a spatially extended Faraday wave state, extending from small amplitudes [states labeled (iii) in Fig. 6] and terminating near the fold of the extended state [states labeled (i)], thereby allowing the extended state to acquire stability [Figs. 6(b), 6(d), and 6(f)]. Note that detuning ($\nu \neq 0$) is not necessary for this behavior. Our model suggests that the localized states shown in Figs. 2(b) and 2(d) lie on connected intertwined branches with stable odd and even states separated by unstable states as in Fig. 6(a).

V. DISCUSSION

In this paper we have reported the observation of slanted snaking of spatially localized structures in a Faraday wave experiment. The experiment was performed in a Hele-Shaw geometry resulting in a quasi-one-dimensional system. The experiments reveal a large parameter region with hysteresis between the flat interface and an extended Faraday wave state. The localized states are found within this region, but extend below the fold in the branch of extended states. This fact, together with the unambiguous slant, indicates that the dynamics of the system are substantially affected by a conserved quantity [27]. We have argued that the most plausible conserved quantity is the liquid volume that is trapped within the oscillating meniscus at the front and back walls of the cell. As the localized wave oscillates, resulting in an oscillation in the number of crests and troughs, liquid is periodically expelled and sucked into the meniscus. We argued that the volume of liquid involved is *independent* of the length of the localized structure and hence that it is a property of the fronts on either side of the structure that connect it to the background flat interface. As a result, the impact of the constraint imposed by the conserved quantity does not decrease with increasing length of the cell (for fixed structure length), in qualitative distinction from other systems of this type [36]. This prediction could in principle be tested in future experiments in order to distinguish this process from the effect of a wave setup that does depend on the length of the cell. However, since the liquid volume trapped in the meniscus is relatively small, we expect the coupling to the large-scale mode to be quite weak already, a conclusion supported by the rather narrow region within which localized Faraday waves are found in the experiment.

In order to model the effect of this conserved quantity on the dynamics of the Faraday waves we constructed a pair of envelope equations, one for the amplitude of the standing Faraday waves themselves, with the other describing the generation of the large-scale mode by spatial inhomogeneities in the wave amplitude, i.e., by the fronts on either side of the structure. This model captures faithfully both the observed inclination of the branch of localized states and the presence of these states outside the hysteresis loop between the flat interface and the spatially extended Faraday wave state. However, a model of this type cannot capture the pinning between the Faraday waves and the fronts and hence cannot capture true snaking of localized states, which requires pinning [4,7]. To incorporate the effects of pinning we generalized the envelope equations by building into the model the natural spatial scale of the waves themselves. This led us to a second model, where the envelope equation for the waves is replaced by a parametrically forced complex Swift-Hohenberg equation coupled to a conserved quantity. This second model captures successfully the distinction between states with odd and even numbers of crests, and their slanted snaking. We believe that both models are of considerable interest, for two reasons: (i) They describe qualitatively but successfully the behavior

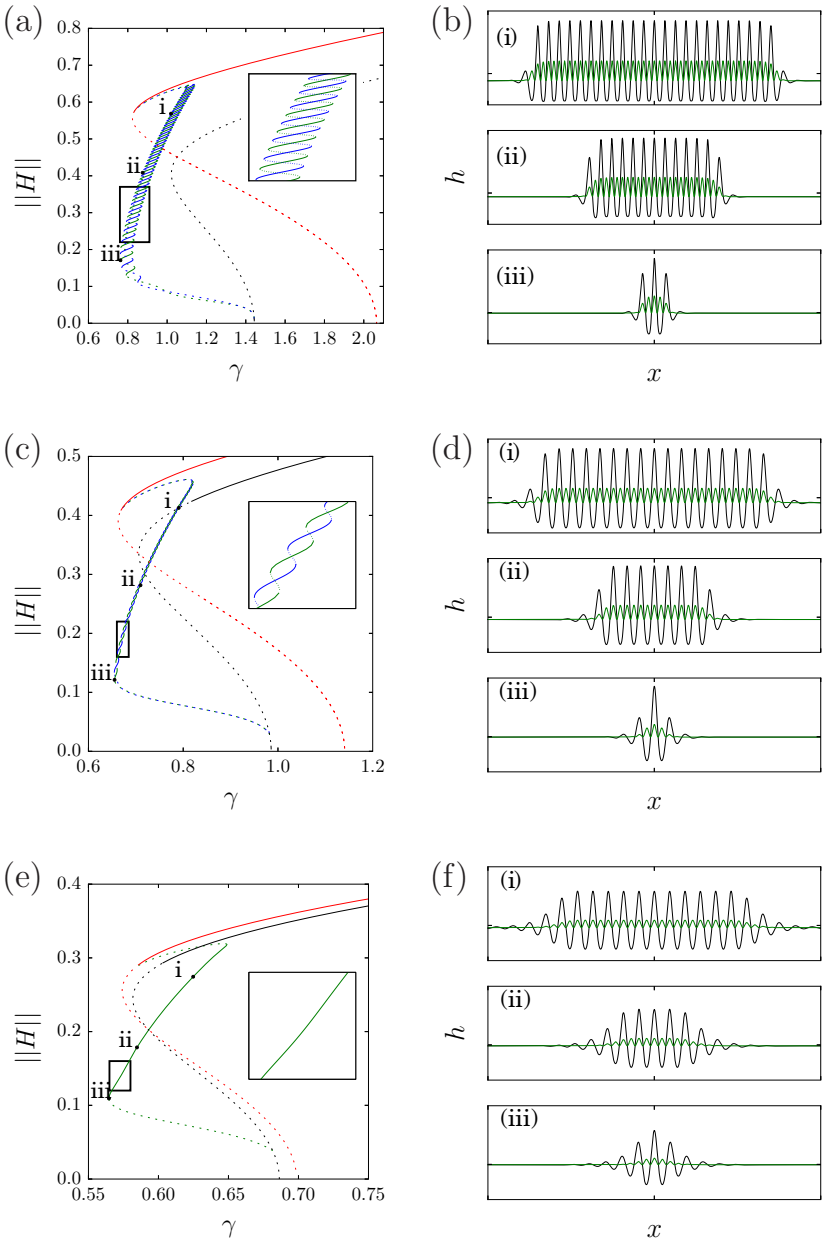

FIG. 6. (a), (c), and (e) Numerical bifurcation diagrams showing time-independent solutions of Eqs. (5) and (3). The black curve represents the primary branch of domain-filling Faraday waves. Localized states (odd, green; even, blue) bifurcate simultaneously at small amplitude, extend beyond the fold, and exhibit slanted snaking before terminating simultaneously on a different branch of domain-filling Faraday waves (red) (cf. [36]). Solid (dotted) lines indicate stable (unstable) solutions. (b), (d), and (f) Profiles of the elevation $h(x,t) = h_0 + B + H\exp(i\omega t/2) + \text{c.c.}$ (black) and the conserved mode B (green) for odd states at $t = 0$ at labeled locations in (a). Panel (e) shows that for smaller values of the parameter ζ slanted snaking is replaced by smooth snaking (only odd localized states are shown). The parameters are $\mu = -0.5$, $\nu = 0$, $\alpha = 1$, $\beta = -4$, $\delta = 1$, $\sigma = 0$, $k_c = 1$, and (a) and (b) $\zeta = 2$, (c) and (d) $\zeta = 1$, and (e) and (f) $\zeta = 0.5$.

of a complex fluid system and (ii) neither model has yet been studied in the applied mathematics literature as a generic model describing the dynamics arising from a parametric instability coupled to a conserved quantity. We leave such studies to future work, while being fully cognizant of the complexity of behavior that these models describe [31].

We have made a preliminary exploration of the two models put forward to explain the experimental observations and showed that with a suitable choice of parameters both models can reproduce the observations. Of course, a more complete theory would seek to derive such models from first principles. In the present case such a derivation would require the solution of the three-dimensional Navier-Stokes equation with a free boundary and moving contact line along the front and back of the Hele-Shaw cell. In the absence of a reliable model of dynamic contact angle motion such a computation is impractical, although we believe that the model (2) and (3) is in principle derivable from first principles, provided the wave amplitude remains small and the group velocity is negligible. The second model, Eq. (5), is not derivable, however, in the same sense that the Swift-Hohenberg equation is not derivable from the equations describing convection [37], despite the original suggestion that it may be a good model of this system. This is because the equation is fundamentally nonasymptotic. Instead, this equation is to be interpreted as a model equation for the spatial profile of the standing waves themselves, rather than for their envelope. In view of the general success of the Swift-Hohenberg equation as a reliable model of spatially localized phenomena [4] we believe, however, that the model will prove an equally reliable guide to the dynamics of localized Faraday waves.

Localized Faraday oscillations in Newtonian fluids confined in a Hele-Shaw cell have been observed before [38], but their origin and possible snaking behavior were not studied. However, the theoretical interpretation of this observation put forward in [38] is untenable since the velocity potential formulation that is used is only valid for inviscid fluids. The flow in a Hele-Shaw geometry is dominated by viscosity, however, as can be seen from the measured order one threshold for the appearance of Faraday waves (see also [39]). As a result, all the coefficients in a Ginzburg-Landau description are necessarily complex. In addition, one cannot mimic the effect of viscosity by simply adding a linear damping term. This is because oscillatory viscous boundary layers generate vorticity that subsequently diffuses into the interior of the liquid [40]. As a result, even in the nearly inviscid limit, the equations describing the flow outside these boundary layers have to be solved with boundary conditions determined by matching the boundary layer solution to the bulk. The resulting bulk flow consists of two contributions, an inviscid flow and a streaming flow driven by the Reynolds stresses arising from these boundary layers [40]. The presence of this streaming flow has recently been confirmed in experiments and direct numerical simulations by Périnet *et al.* [41]; formulations that include viscous damping but omit these stresses underestimate the magnitude of the streaming flow [42,43]. We mention that the theory suggested in [38] writes down an equation for the amplitude of a $\cos kx$ mode, i.e., a spatially periodic structure that, as shown here, has nothing to do with the observed spatially localized state. Indeed, in strongly dissipative systems the amplitude equation for standing waves takes a form that differs from the parametrically driven Ginzburg-Landau equation [44]. Finally, the primary instability necessarily generates a state that is either odd or even under reflection [45], implying that the rocking structure observed in [38] must be the result of a secondary instability.

In summary, the present experiment reveals a large multiplicity of spatially localized Faraday waves organized in a slanted snaking bifurcation diagram, an observation that can be qualitatively understood using both amplitude equations [Eq. (2)] and a model equation constructed in the spirit of the Swift-Hohenberg model [Eq. (5)], provided volume conservation is taken into account in both cases [Eq. (3)].

ACKNOWLEDGMENTS

The authors acknowledge financial support from CONICYT Grant No. CONICYT-USA PII20150011, FONDECYT Grants No. 1130354 and No. 1150507, and the Berkeley-Chile Fund. The authors thank G. Camel, L. Gordillo, and A. Rucklidge for discussions.

[1] *Localized States in Physics: Solitons and Patterns*, edited by O. Descalzi, M. Clerc, S. Residori, and G. Assanto (Springer, New York, 2011).
[2] H. G. Purwins, H. U. Bödeker, and S. Amiranashvili, Dissipative solitons, Adv. Phys. **59**, 485 (2010).
[3] M. C. Cross and P. C. Hohenberg, Pattern formation outside of equilibrium, Rev. Mod. Phys. **65**, 851 (1993).
[4] E. Knobloch, Spatial localization in dissipative systems, Annu. Rev. Condens. Matter Phys. **6**, 325 (2015).
[5] P. Coullet, C. Riera, and C. Tresser, Stable Static Localized Structures in One Dimension, Phys. Rev. Lett. **84**, 3069 (2000).
[6] M. Beck, J. Knobloch, D. J. B. Lloyd, B. Sandstede, and T. Wagenknecht, Snakes, ladders, and isolas of localized patterns, SIAM J. Math. Anal. **41**, 936 (2009).
[7] Y. Pomeau, Front motion, metastability and subcritical bifurcations in hydrodynamics, Physica D **23**, 3 (1986).
[8] J. Burke, and E. Knobloch, Localized states in the generalized Swift-Hohenberg equation, Phys. Rev. E **73**, 056211 (2006).
[9] J. Burke and E. Knobloch, Homoclinic snaking: Structure and stability, Chaos **17**, 037102 (2007).
[10] W. J. Firth, L. Columbo, and T. Maggipinto, On homoclinic snaking in optical systems, Chaos **17**, 037115 (2007).
[11] S. Barbay, X. Hachair, T. Elsass, I. Sagnes, and R. Kuszelewicz, Homoclinic Snaking in a Semiconductor-Based Optical System, Phys. Rev. Lett. **101**, 253902 (2008).
[12] J. Abshagen, M. Heise, G. Pfister, and T. Mullin, Multiple localized states in centrifugally stable rotating flow, Phys. Fluids **22**, 021702 (2010).
[13] F. Haudin, R. G. Rojas, U. Bortolozzo, S. Residori, and M. G. Clerc, Homoclinic Snaking of Localized Patterns in a Spatially Forced System, Phys. Rev. Lett. **107**, 264101 (2011).
[14] U. Thiele, A. J. Archer, M. J. Robbins, H. Gomez, and E. Knobloch, Localized states in the conserved Swift-Hohenberg equation with cubic nonlinearity, Phys. Rev. E **87**, 042915 (2013).
[15] D. J. B. Lloyd, C. Gollwitzer, I. Rehberg, and R. Richter, Homoclinic snaking near the surface instability of a polarisable fluid, J. Fluid Mech. **783**, 283 (2015).
[16] W. J. Firth, L. Columbo, and A. J. Scroggie, Proposed Resolution of Theory-Experiment Discrepancy in Homoclinic Snaking, Phys. Rev. Lett. **99**, 104503 (2007).
[17] J. H. P. Dawes, Localized pattern formation with a large-scale mode: Slanted snaking, SIAM J. Appl. Dyn. Syst. **7**, 186 (2008).
[18] P. Assemat, A. Bergeon, and E. Knobloch, Spatially localized states in Marangoni convection in binary mixtures, Fluid Dyn. Res. **40**, 852 (2008).
[19] M. G. Clerc, C. Fernández-Oto, and S. Coulibaly, Pinning-depinning transition of fronts between standing waves, Phys. Rev. E **87**, 012901 (2013).
[20] A. S. Alnahdi, J. Niesen, and A. M. Rucklidge, Localized patterns in periodically forced systems, SIAM J. Appl. Dyn. Sys. **13**, 1311 (2014).
[21] M. Faraday, On a peculiar class of acoustical figures; and on certain forms assumed by groups of particles upon vibrating elastic surfaces, Philos. Trans. R. Soc. London **121**, 299 (1831).
[22] O. del Rio and A. W. Neumann, Axisymmetric drop shape analysis: Computational methods for the measurement of interfacial properties from the shape and dimensions of pendant and sessile drops, J. Colloid Interface Sci. **196**, 136 (1997).
[23] P. G. de Gennes, Wetting: statics and dynamics, Rev. Mod. Phys. **57**, 827 (1985).
[24] J. E. Macías, M. G. Clerc, C. Falcón, and M. A. García-Ñustes, Spatially modulated kinks in shallow granular layers, Phys. Rev. E **88**, 020201(R) (2013).
[25] C. Beaume, H.-C. Kao, E. Knobloch, and A. Bergeon, Localized rotating convection with no-slip boundary conditions, Phys. Fluids **25**, 024105 (2013).
[26] J. H. P. Dawes and S. Lilley, Localized states in a model of pattern formation in a vertically vibrated layer, SIAM J. Appl. Dyn. Syst. **9**, 238 (2010).
[27] E. Knobloch, Localized structures and front propagation in systems with a conservation law, IMA J. Appl. Math. **81**, 457 (2016).
[28] P. C. Matthews and S. M. Cox, Pattern formation with a conservation law, Nonlinearity **13**, 1293 (2000).

[29] S. M. Cox and P. C. Matthews, New instabilities in two-dimensional rotating convection and magnetoconvection, Physica D **149**, 210 (2001).
[30] P. Coullet and G. Iooss, Instabilities of One-Dimensional Cellular Patterns, Phys. Rev. Lett. **64**, 866 (1990).
[31] J. Burke, A. Yochelis, and E. Knobloch, Classification of spatially localized oscillations in periodically forced dissipative systems, SIAM J. Appl. Dyn. Syst. **7**, 651 (2008).
[32] H.-C. Kao and E. Knobloch, Weakly subcritical stationary patterns: Eckhaus instability and homoclinic snaking, Phys. Rev. E **85**, 026211 (2012).
[33] G. Kozyreff and S. J. Chapman, Asymptotics of Large Bound States of Localized Structures, Phys. Rev. Lett. **97**, 044502 (2006).
[34] B. A. Malomed, Nonlinear waves in nonequilibrium systems of the oscillatory type, Part I, Z. Phys. B **55**, 241 (1984).
[35] L. Gelens and E. Knobloch, Traveling waves and defects in the complex Swift-Hohenberg equation, Phys. Rev. E **84**, 056203 (2011).
[36] D. Lo Jacono, A. Bergeon, and E. Knobloch, Magnetohydrodynamic convectons, J. Fluid Mech. **687**, 595 (2011).
[37] Y.-P. Ma and E. A. Spiegel, A diagrammatic derivation of (convective) pattern equations, Physica D **240**, 150 (2011).
[38] J. Rajchenbach, A. Leroux, and D. Clamond, New Standing Solitary Waves in Water, Phys. Rev. Lett. **107**, 024502 (2011).
[39] K. Kumar and L. S. Tuckerman, Parametric instability of the interface between two fluids, J. Fluid Mech. **279**, 49 (1994).
[40] J. M. Vega, E. Knobloch, and C. Martel, Nearly inviscid Faraday waves in annular containers of moderately large aspect ratio, Physica D **154**, 313 (2001).
[41] N. Périnet, P. Gutiérrez, H. Urra, N. Mujica, and L. Gordillo, Streaming patterns in Faraday waves, J. Fluid Mech. **819**, 285 (2017).
[42] O. M. Phillips, *The Dynamics of the Upper Ocean*, 2nd ed. (Cambridge University Press, Cambridge, 1980).
[43] E. Knobloch and J. M. Vega, in *Geometry, Mechanics and Dynamics*, edited by P. Newton, P. Holmes, and A. Weinstein (Springer, Berlin, 2002), pp. 181–222.
[44] A. M. Rucklidge and M. Silber, Design of parametrically forced patterns and quasipatterns, SIAM J. Appl. Dyn. Syst. **8**, 298 (2009).
[45] J. D. Crawford and E. Knobloch, Symmetry and symmetry-breaking bifurcations in fluid mechanics, Annu. Rev. Fluid Mech. **23**, 341 (1991).